Nuclear Model Calculations below 200 MeV and Evaluation Prospects

Arjan Koning

Netherlands Energy Research Foundation ECN, P.O. Box 1, 1755 ZG Petten, The Netherlands

Olivier Bersillon and Jean-Paul Delaroche

Service de Physique et Techniques Nucléaires, CEA, B.P 12, F-91680 Bruyères-le-Châtel, France

Abstract

A computational method is outlined for the quantum-mechanical prediction of the whole double-differential energy spectrum. Cross sections as calculated with the code system MINGUS are presented for (n,xn) and (p,xn) reactions on ^{208}Pb and ^{209}Bi. Our approach involves a dispersive optical model, comprehensive discrete state calculations, renormalized particle-hole state densities, a combined MSD/MSC model for pre-equilibrium reactions and compound nucleus calculations. The relation with the evaluation of nuclear data files is discussed.

1 Introduction

Light-particle induced nuclear reactions above 10 MeV can be categorized as follows:

- elastic scattering and direct reactions to collective discrete states [1], analyzed with the optical model and DWBA or coupled channels models. Giant resonances also belong to this class.
- pre-equilibrium reactions [2], analyzed with semi-classical exciton and hybrid models or quantum-mechanical multi-step direct/multi-step compound models.
- equilibrium reactions to the continuum [2], analyzed with the classical Weisskopf-Ewing model or the quantum-mechanical Hauser-Feshbach model.

As is now well known, the pre-equilibrium reaction mechanism constitutes the bridge between fast, direct processes and slow, compound processes and provides an explanation for the observed high-energy tails in spectra and the smoothly forward peaked angular distributions. In the past (and also in the Intermediate Energy Code Comparison [3]), pre-equilibrium reactions have been analyzed mainly with semi-classical exciton models and hybrid models which, while not being based on first principles, provide a reasonably good description of the continuum high-energy tail of nuclear reaction spectra. The advent of more rigorous pre-equilibrium theories, such as that of Feshbach, Kerman and Koonin [4], and the simultaneous development of fast computers, enabled to perform quantum-mechanical pre-equilibrium calculations. After pioneering work of Tamura et al. [5] and Bonetti et al. [6], there has now been reached a scientifically healthy situation with several independent implementations of both multi-step direct (MSD) and multi-step compound (MSC) models. Although several controversies about both theoretical (such as causality problems in the MSD theory [7, 8]) and practical aspects still exist, there is nevertheless a tendency that quantum-mechanical pre-equilibrium models explain the experimental double-differential data better than the classical models. Eventually, they may replace the latter if the systematic behavior of the remaining adjustable parameter(s) is under control. The two most important generalizations of the present quantum-mechanical pre-equilibrium models that are still required are multiple pre-equilibrium emission (which is currently being investigated [9]) and a general description of complex particle emission.
There have been several computational analyses of nuclear reaction spectra that include more than one of the reaction mechanisms mentioned in the beginning (for example, the unified exciton model for pre-equilibrium/equilibrium processes), often with omission or a semi-phenomenological description of the remainder (usually the collective part). Up to now, there has been no consistent integrated quantum-mechanical approach that treats all aforementioned reaction types on an equal footing. As a first step in that direction, we present here a complete quantum-mechanical prediction of the whole outgoing double-differential energy spectrum of a nucleon-induced reaction. We believe that an essential *theoretical* aspect of such a description is, besides the reaction dynamics, a consistent use of both adequate optical models and level density prescriptions in all partial reaction models and that the essential *practical* aspect is that these reaction models are implemented in one computer code. The calculations we present here are performed with the computer code MINGUS, which calculates MSD, MSC and compound cross sections and combines these with elastic and collective cross sections as provided by ECIS88 [10], yielding complete double-differential outgoing spectra in one single

run. All basic transition amplitudes and cross sections that are necessary for the MSD, MSC and compound models are also computed by ECIS88. MINGUS is the extension of, and has the same modular structure as, the multi-step direct code KAPSIES [11] that has been used in the Comparison for (p,p') reactions below 200 MeV.
Within the scope of the Comparison, we present here our recent results for several nucleon induced reactions on ^{208}Pb and ^{209}Bi. First, we give an outline of the neutron dispersive optical model that we use throughout this work and test it against experimental total cross sections and several differential elastic and inelastic measurements. Next, we discuss our discrete level calculations, level densities and the continuum reaction models. We establish the contribution of all reaction mechanisms by analyzing precisely measured double-differential 14 MeV (n,xn) spectra and subsequently we proceed with higher incident energies. Finally, we indicate how our calculations can be used for nuclear data evaluation above 20 MeV.

2 The dispersive optical model

In recent years, the theory of the nuclear optical model has been reformulated in terms of dispersion relations that connect the real and imaginary parts of the optical potential. These dispersion relations are a natural result of the causality principle that a scattered wave cannot be emitted before the arrival of the incident wave. For the theoretical details we refer to [12, 13, 14]. Here, we restrict ourselves to the essential points that are necessary to perform practical calculations with the dispersive optical model.
The phenomenological optical model potential U has the following form:

$$\begin{aligned} U(r,E) &= -V(E)f_v(r) + 4ia_{w_D}W_D(E)\frac{\mathrm{d}f_{w_D}(r)}{\mathrm{d}r} - iW(E)f_w(r) \\ &+ \left(\frac{\hbar}{m_\pi c}\right)^2 \mathbf{l}.\sigma V_{so}(E)\frac{1}{r}\frac{\mathrm{d}f_{so}(r))}{\mathrm{d}r} + V_C(r), \end{aligned} \tag{1}$$

where $f_\mu(r)$ represents the Woods-Saxon shape

$$\begin{aligned} f_\mu(r) &= \frac{1}{1+\exp((r-R_\mu)/a_\mu)}, \\ R_\mu &= r_\mu A^{1/3}, \end{aligned} \tag{2}$$

where a_μ and R_μ are the diffuseness and radius of each component μ. In the dispersive optical model, a real volume component, ΔV_v, and real surface potential, V_D, (the latter is usually zero in a conventional optical model potential) are connected to the imaginary volume, W, and surface, W_D, components by means of the dispersion relations

$$\Delta V_v(E) = \frac{\mathcal{P}}{\pi}\int_{-\infty}^{\infty}\frac{W(E')}{E'-E}dE', \qquad V_D(E) = \frac{\mathcal{P}}{\pi}\int_{-\infty}^{\infty}\frac{W_D(E')}{E'-E}dE'. \tag{3}$$

If one assumes that the geometry of the real and imaginary volume parts are the same, the real volume potential of Eq. (1) can be written as the sum of the Hartree-Fock potential and the extra volume component

$$V(E) = V_H(E) + \Delta V_v(E). \tag{4}$$

In general, Eqs. (3) cannot be solved analytically. However, under the reasonable assumption [12] that the imaginary potential is symmetric with respect to the Fermi energy E_F (which is

defined as the energy halfway the last occupied and the first unoccupied shell), we can rewrite the dispersion relation as

$$\mathcal{V}(E) = \frac{2}{\pi}(E - E_F)\mathcal{P}\int_{E_F}^{\infty} \frac{\mathcal{W}(E')}{(E' - E_F)^2 - (E - E_F)^2} dE'. \tag{5}$$

This equation holds for either the surface or volume term. Following Delaroche [15], we can give the analytical solution for two special, frequently occurring, cases. Let $z = E - 2E_F$. Then

a/ The imaginary potential has the form

$$\begin{aligned} E_F < E < E_a &: \mathcal{W}(E) = 0 \\ E_a < E < E_b &: \mathcal{W}(E) = g(E - E_a) \\ E_b < E < \infty &: \mathcal{W}(E) = g(E_b - E_a). \end{aligned} \tag{6}$$

Usually, this form occurs for the imaginary volume potential W. With Eq. (5) we obtain for the real potential

$$\begin{aligned} \mathcal{V}(E) &= \frac{g}{\pi}[(E - E_a)\log\left|\frac{E_b - E}{E_a - E}\right| + (E_a + z)\log\left(\frac{E_b + z}{E_a + z}\right) \\ &+ (E_b - E_a)\log\left|\frac{E_b + z}{E_b - E}\right|]. \end{aligned} \tag{7}$$

b/ The imaginary potential has the form

$$\begin{aligned} E_F < E < E_a &: \mathcal{W}(E) = a_1(E - E_F) \\ E_a < E < E_b &: \mathcal{W}(E) = b_1(E_b - E) \\ E_b < E < \infty &: \mathcal{W}(E) = 0. \end{aligned} \tag{8}$$

Usually, this form occurs for the imaginary surface potential W_D. With Eq. (5) we obtain for the real potential

$$\begin{aligned} \mathcal{V}(E) &= \frac{a_1}{\pi}(E - E_F)\left[\log|(E_a - E)(E_a + z)| - 2\log|E - E_F|\right] \\ &+ \frac{b_1}{\pi}\left[(E_b - E)\log\left|\frac{E_b - E}{E_a - E}\right| + (E_b + z)\log\left(\frac{E_a + z}{E_b + z}\right)\right]. \end{aligned} \tag{9}$$

A result of the dispersion relation formalism is that in the presence of an imaginary surface potential, the optical model potential (1) is extended with a real surface term

$$V_D = 4a_{v_D}V_D(E)\frac{\mathrm{d}f_{v_D}(r)}{\mathrm{d}r}. \tag{10}$$

The two cases a/ and b/ apply to the neutron optical model that we adopt for ^{208}Pb. We use the optical model parameters of Johnson et al. [16] together with the aforementioned dispersion relations.
The parameters for the Hartree-Fock potential are

$$V_H(E) = 46.4\exp(-0.31(E - E_F)/46.4)\,\mathrm{MeV},\ \ r_{v_H} = 1.24\,\mathrm{fm},\ \ a_{v_H} = 0.68\,\mathrm{fm}, \tag{11}$$

with Fermi energy $E_F = -6$ MeV.

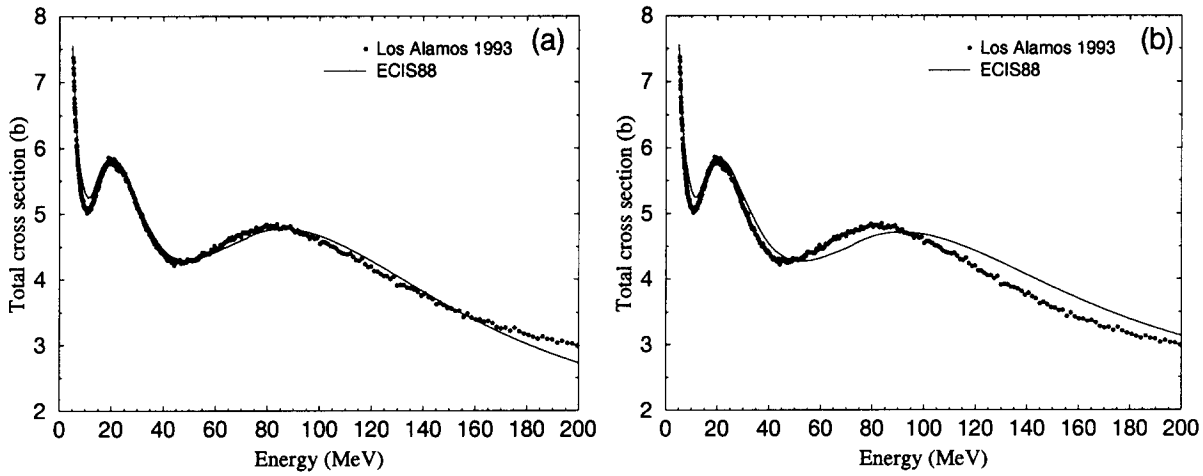

Figure 1: Total neutron cross section for ^{208}Pb as calculated with ECIS88: (a) Non-relativistic case , (b) Relativistic case. The experimental data are from [17].

The imaginary volume potential and geometry are parametrized as

$$\begin{aligned} E < 10 \text{ MeV} &: W(E) = 0 \\ 10 < E < 50 \text{ MeV} &: W(E) = 0.17(E - 10) \text{ MeV} \\ E > 50 \text{ MeV} &: W(E) = 6.8 \text{ MeV} \\ r_w = 1.24 \text{ fm} &, \quad a_w = 0.68 \text{ fm}. \end{aligned} \tag{12}$$

Using Eq. (7), the extra real volume component of Eq. (4) can be calculated.
The imaginary surface potential and geometry are given by:

$$\begin{aligned} E < 10 \text{ MeV} &: W_D(E) = 0.4(E - E_F) \text{ MeV} \\ 10 < E < 72 \text{ MeV} &: W_D(E) = -0.103(E - 72) \text{ MeV} \\ E > 72 \text{ MeV} &: W_D(E) = 0 \\ r_{w_D} = 1.27 \text{ fm} &, \quad a_{w_D} = 0.58 \text{ fm}. \end{aligned} \tag{13}$$

Using Eq. (9), the real surface contribution V_D can be calculated.
The spin-orbit parameters are

$$V_{so} = 5.75 \text{ MeV}, \quad r_{so} = 1.105 \text{ fm}, \quad a_{so} = 0.50 \text{ fm}. \tag{14}$$

This parametrization results in a single dispersive optical model for neutrons that gives good agreement with measured total and elastic scattering cross sections from several keV up to 165 MeV. In fig. 1(a) we have displayed a comparison between the total cross sections as calculated by ECIS88 and recent experimental data [17]. We stress that the analysis by Johnson et al. was performed without taking into account relativistic kinematics. To indicate the significance of this, we have displayed in fig. 1(b) the calculated results including relativistic effects. It is obvious that a re-tuning of the optical model parameters is required if one turns to a relativistic description. An additional serious option for improvement would be to replace, for all energies [18], the Schrödinger equation by the Dirac equation in the optical model calculations. In this work, however, we restrict ourselves to the combination of the dispersive optical model with parameters as given in (11-14) and non-relativistic kinematics.
In fig. 2, we have depicted the elastic cross section for several energies. Without exception, there is excellent agreement with measured elastic angular distributions, also at energies above

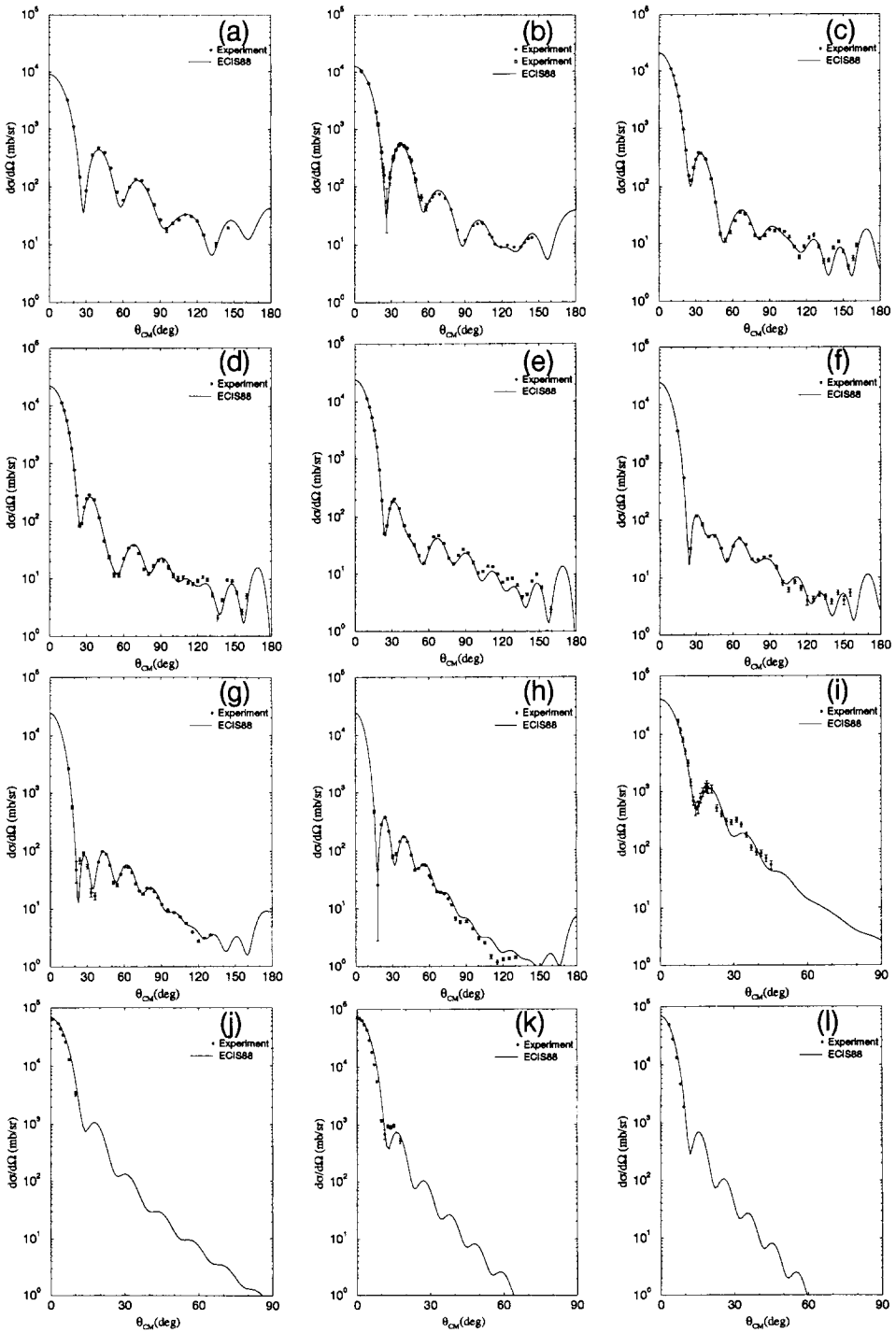

Figure 2: Differential cross sections for neutron elastic scattering on ^{208}Pb at (a) 11 MeV, (b) 14 MeV, (c) 20 MeV, (d) 22 MeV, (e) 24 MeV, (f) 26 MeV, (g) 30 MeV, (h) 40 MeV, (i) 65 MeV, (j) 96 MeV, (k) 136 MeV and (l) 155 MeV. The calculations were performed with ECIS88 using the optical model parameters by Johnson et al. [16].

40 MeV which were not published in [16]. The conclusion is that for neutrons on ^{208}Pb there is a unique optical model that predicts the total and the elastic scattering cross sections with good accuracy. The relevance of this in the present work is that we can safely rely on this optical model for the prediction of double-differential reaction spectra involving neutron energies up to 150 MeV.
For protons, we use the parametrization of [19], which is also reliable up to at least 150 MeV.

3 Direct reactions to discrete states

After establishing the optical model, we can start with the description of the inelastic reactions to discrete states. We aim at a full treatment of collective effects. Therefore, in order not to miss any collective strength, our calculation includes 70 discrete levels of ^{208}Pb for which the spin, parity and deformation lengths δ_L are known. In this way, we avoid a simulation of the collective part of the spectrum by the continuum MSD mechanism. For each level, we performed a DWBA vibrational model calculation with ECIS88. The discrete state parameters were obtained from a 35 MeV proton inelastic scattering analysis by Wagner et al. [20]. Since the deformation parameters β_L of Ref. [20] were obtained with the help of the Becchetti-Greenlees optical potential, which does not contain a real surface term, we have transformed the dispersive optical model into a form without a real surface potential. This can be accomplished by adding the real surface term (9) to the real volume term (4). Then, one can construct an equivalent form of the original dispersive optical model that contains an energy-dependent radius for a modified effective real volume potential. This is a necessary operation before one can perform a consistent transformation of the deformation parameters of [20] into deformation lengths and vice versa for inelastic scattering at another incident energy. Formally, for the deformation length of each level we have

$$\begin{aligned} \delta_L &= \beta_L^{BG}.R^{BG} \\ &= \beta_L^{\mathrm{real}}(E).R^{\mathrm{real}}(E) \\ &= \beta_L^{\mathrm{imag}}(E).R^{\mathrm{imag}}(E), \end{aligned} \tag{15}$$

where β_L^{BG} and R^{BG} are the deformation parameter and (Becchetti-Greenlees) radius from Ref. [20] and the other quantities are associated with an inelastic scattering at an incident energy E. Note that this relationship holds for both the real and the imaginary part of the potential. In our calculations with ECIS88, the deformation lengths are automatically transformed to deformation parameters for each different component of the optical potential.
To test this procedure, we have compared DWBA calculations at 11 and 25.7 MeV neutron inelastic scattering on ^{208}Pb for the first 3^- and 5^- states with experiment [21]. Figure 3 shows that the deformation lengths as inferred from the 35 MeV (p,p') reaction of Ref. [20] result in a good prediction of the inelastic angular distribution. Adjustment of the deformation parameters may lead to an even better agreement [22], especially for low incident energies (for which a coupled channels calculation may be more appropriate [23]), but here we do not address to this since we merely want to demonstrate the global predictive power of our approach.
Given the succes of predicting the cross sections corresponding to the first 3^- and 5^- state, we can compare the calculated cross sections for all 70 states with experimental double-differential spectra. This can be achieved by simulating the experimental spreading and the spreading of the spectroscopic strength by a Gaussian broadening of the cross section for each state. We fix the width of this Gaussian at the elastic peak. Then, if the experiment is of a time-of-flight

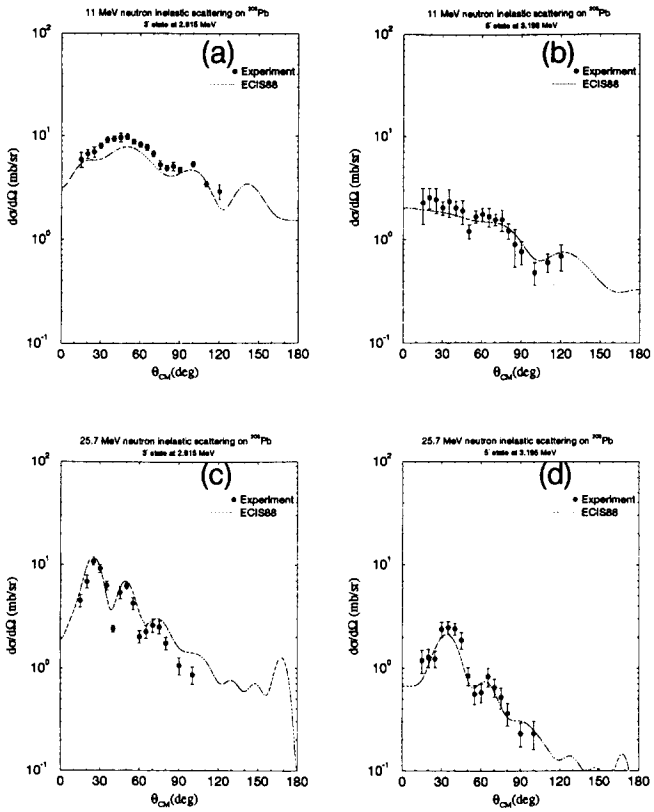

Figure 3: Differential inelastic cross section for neutrons on ^{208}Pb at (a-b) 11 MeV, (c-d) 25.7 MeV, using DWBA calculations by ECIS88 and deformation lengths derived from [20].

nature (which is the case for the (n,n') reactions we study in this paper) and the spreading of the experimental resolution is much larger than the spectroscopic spreading, the width decreases as $E^{3/2}$ for lower outgoing energies.

By including this broadening of the discrete states one can perform an accurate investigation of the overlap of the smooth MSD region, basically of a single-particle nature, and the more structured collective region. Only hereafter, one can can draw meaningful conclusions on the MSD contribution and its associated parameters. In some previous analyses of (pre-equilibrium) reactions to the continuum, the collective part of the spectrum was predicted by a closed-form formula [24] for the angle-integrated cross sections for the first 2^+ and 3^- state. Recently, there has been evidence [25, 26] that this closed-form expression fails to give consistent good results upon varying incident energy. The calculations displayed in section 9 show that our complete DWBA approach solves this problem and in addition provides an adequate description of the fluctuations in the high-energy tail at all angles.

It is obvious that the inclusion of an extensive discrete level scheme in the calculations for the high-energy tail enables a reliable estimate of the compound formation cross section (defined as the total reaction cross section minus the integrated collective and MSD cross section). This is essential for a precise calculation of the MSC and compound contribution.

4 Level density

For the description of reactions to the continuum, we aim at a consistent use of level density prescriptions for both the pre-equilibrium and equilibrium models. A major role in level density models is played by the level density parameter a. The parametrization $a = A/k$ MeV^{-1} (where $k \sim 8$), which is frequently employed in pre-equilibrium calculations, is not adequate in the neighborhood of magic nuclei and certainly not for the ^{208}Pb and ^{209}Bi nuclei we study here. Instead, marked shell effects appear for these nuclei and these effects manifest themselves by an associated decrease of the level density parameter at the binding energy [27]. It has been argued by Ignatyuk et al. [28] that these shell effects disappear with increasing excitation energy so that at sufficiently high excitation energy a simple linear mass dependence of the level density parameter is recovered. To incorporate the shell effects in our calculations, we have adopted the parametrization of Ignatyuk et al. for the level density parameter a as a function of the excitation energy E_x:

$$a(E_x) = \tilde{a}(1 - \frac{f(E_x)\delta W}{E_x}), \tag{16}$$

where δW is the shell correction to the mass formula of Myers-Swiatecki [29] and $\tilde{a}$ is the asymptotic value of a at high excitation energies, parametrized as

$$\frac{\tilde{a}}{A} = \alpha + \beta A, \tag{17}$$

where $\alpha = 0.154$ MeV^{-1} and $\beta = -6.3.10^{-5}$ MeV^{-1}. The function $f(E_x)$ is given by

$$f(E_x) = 1 - \exp(-\gamma E_x), \tag{18}$$

where $\gamma = 0.054$ MeV^{-1}. In fig. 1 of Ref. [28] the correspondence between the level density parameter at the binding energy and the shell corrections is displayed. This stimulated us to eliminate δW from Eq. (16) by imposing the boundary condition that at the binding energy the level density parameter as deduced from Eq. (16) must coincide with a value determined from a conventional, energy-independent analysis. Also, Ignatyuk et al. observed that extrapolating Eq. (16) to too low excitation energies may be dubious, which motivated us to keep the level density parameter constant below the neutron binding energy B. Together, this leads to the following parametrization of the energy-dependent level density parameter:

$$\begin{aligned} a(E_x) &= a_B \qquad\qquad\qquad\qquad , \text{ if } E_x < B \\ &= \tilde{a}(1 - \frac{f(E_x)B(1 - a_B/\tilde{a})}{f(B)E_x}), \text{ if } E_x > B, \end{aligned} \tag{19}$$

where a_B, being the level density parameter at the neutron binding energy, may be taken from a standard level density table. We employ the same energy dependent level density parameter $a(E_x)$ in both the partial and total level density formula.
For the total level density we take the backshifted Fermi gas prescription [30] given by

$$\omega(E_x) = \frac{\sqrt{\pi}}{12} \frac{\exp(2\sqrt{(a(E_x - \Delta))})}{a^{1/4}(E_x - \Delta + t)^{5/4}}, \tag{20}$$

where Δ is the pairing correction and the nuclear temperature t is given by

$$E_x - \Delta = at^2 - t. \tag{21}$$

The distribution of the nuclear states with spin J is given by

$$R(J) = \frac{2J+1}{2\sigma^2} \exp\left[-\frac{(J+\frac{1}{2})^2}{2\sigma^2}\right], \tag{22}$$

where σ is the spin cutoff factor.
For our pre-equilibrium calculations, we start with the Williams formula [31] for the partial state density for p particles and h holes and in addition employ two extensions of this expression. Firstly, Williams has shown that summing his combinatorial formula over all particles and holes leads to a total level density formula with a U^{-1} dependence whereas the commonly used total level density formulae such as Eq. (20) show a $U^{-5/4}$ dependence. Therefore, we follow Akkermans and Gruppelaar [32] by adopting a renormalization of the Williams formula, such that upon summation over all particle and holes it coincides with the backshifted Fermi gas formula (20). This ensures more consistency when performing both pre-equilibrium and equilibrium calculations. Secondly, we adopt Oblozinsky's generalization [33] of the Williams formula, which takes the finite depth of the hole into account and enables to distinguish between bound and unbound particle-hole configurations. These extensions lead to the following general form for the particle-hole state density:

$$\begin{aligned} \omega_{p,h}(E_x) &= f(E_x)\frac{g^n}{p!h!(n-1)!}\sum_{i=0}^{p}\sum_{j=0}^{h}(-1)^{i+j}\binom{p}{i}\binom{h}{j} \\ &\times (E_x - \Delta - A_{p,h} - iB - jF)^{n-1}\Theta(E_x - \Delta - E_{PP} - iB - jF). \end{aligned} \tag{23}$$

Here, F is the Fermi energy, B is the binding energy, $E_{PP} = [p^2+h^2+p-h]/2g$ is the minimum energy required to excite p particles and h holes satisfying the Pauli principle, Θ is the unit step function, $g = \frac{6a}{\pi^2}$ is the (energy-dependent) single-particle state density, $n = p+h$ is the exciton number and $A_{p,h} = [p(p-1)+h(h-1)]/4g$ is the Pauli correction factor. The function $f(E_x)$ is given by [32]

$$f(E_x) = (\frac{\pi}{3})^{1/2}\frac{(E_x - \Delta)}{a^{1/4}(E_x - \Delta + t)^{5/4}}. \tag{24}$$

For MSC calculations, we use exactly Eq. (23) and for MSD we use Eq. (23) with $B \to \infty$. The distribution of the particle-hole states with spin J is given by

$$R_n(J) = \frac{2J+1}{\pi^{1/2}n^{3/2}\sigma^3} \exp\left[-\frac{(J+\frac{1}{2})^2}{n\sigma^2}\right]. \tag{25}$$

5 Multi-step direct reactions

For excitation energies above a few MeV, it is no longer possible to distinguish between isolated excited states. A natural extension of discrete direct reactions to the continuum part of the spectrum is then provided by the multi-step direct (MSD) mechanism. Again, for relatively high outgoing energies, the reaction proceeds by a direct-like reaction mechanism. In this case however, the high level density of the residual nucleus necessitates statistical postulates in order to obtain practicable formulae for the analysis of these processes. When a reaction proceeds by the MSD mechanism, it is imagined that at least one particle is in the continuum and that at each subsequent step of the reaction a new particle-hole pair is created. After one or a few steps, the continuum particle is emitted in a direction that is still coupled to the initial direction. This, together with the high density of states, explains the observed

(energy averaged) smooth forward peaked angular distributions (for examples, see [2]). The three most prominent MSD theories are those of Feshbach, Kerman and Koonin (FKK) [4], Tamura, Udagawa and Lenske [5] and Nishioka, Weidenmüller and Yoshida [34]. A study of both the theoretical [35] and practical [11] aspects of the models revealed that the FKK model, because of a strong statistical assumption that we called leading-particle statistics, is conceptually and computationally the most attractive. Furthermore, we concluded that, despite their considerable conceptual differences concerning the quantum-statistical assumptions, the three models appear to have essentially the same predictive power with respect to double-differential cross sections. Thus, we argued that the FKK model is the most appropriate tool for nuclear data calculations. In [8, 11], we presented a compact form of the FKK MSD cross section that lends itself easily for implementation. It reads

$$\frac{d^2\sigma(E_k,\Omega \leftarrow E_{k_0},\Omega_0)}{d\Omega dE_k} = \sum_{n=1}^{\infty} \frac{d^2\sigma^{(n)}(E_k,\Omega \leftarrow E_{k_0},\Omega_0)}{d\Omega dE_k}. \tag{26}$$

The first step cross section is given by

$$\frac{d^2\sigma^{(1)}(E_k,\Omega \leftarrow E_{k_0},\Omega_0)}{d\Omega dE_k} = \sum_J (2J+1) R_n(J) \omega_{1p1h}(E_x) \left[\frac{d\sigma(E_k,\Omega \leftarrow E_{k_0},\Omega_0)}{d\Omega}\right]_J^{DWBA}, \tag{27}$$

and the n-step ($n > 1$) cross section can be written in the following recursive form:

$$\begin{aligned} \frac{d^2\sigma^{(n)}(E_k,\Omega \leftarrow E_{k_0},\Omega_0)}{d\Omega dE_k} &= \frac{m}{4\pi^2\hbar^2} \int \mathrm{d}\Omega_{n-1} \int \mathrm{d}E_{k_{n-1}} E_{k_{n-1}} \\ \times \quad & \frac{d^2\sigma^{(1)}(E_k,\Omega \leftarrow E_{k_{n-1}},\Omega_{n-1})}{d\Omega dE_k} \frac{d^2\sigma^{(n-1)}(E_{k_{n-1}},\Omega_{n-1} \leftarrow E_{k_0},\Omega_0)}{d\Omega_{n-1} dE_{k_{n-1}}}. \end{aligned} \tag{28}$$

By definition, there is always at least one continuum particle in the MSD chain. Hence, the total system is always unbound and the level density that appears in Eq.(27) is given by Eq.(23) with $B \rightarrow \infty$ and is restricted only by the finite depth of the hole. The quantities between brackets in Eq. (27) are DWBA cross sections for each transferred angular momentum. In order to maintain consistency with our discrete reaction calculations, we followed the same macroscopic DWBA approach, only this time with much smaller, l-independent deformation parameters (see [5, 11] for a discussion of this procedure).

We prevent double counting of collective and MSD contributions by subtracting the averaged collective cross section from the MSD cross sections. This entails that if the discrete level scheme of a nucleus is well documented in terms of level energy, spin, parity and deformation length, we can extend our collective state calculations up to several MeV of excitation energy, and the effective MSD contribution enters only gradually after a few MeV. This is the case for the ^{208}Pb and ^{209}Bi nuclei we consider here.

6 Multi-step compound reactions

Multi-step compound (MSC) reactions occur at somewhat higher energies than those characteristic of compound nucleus decay. In the MSC reaction mechanism, the stepwise reaction proceeds exclusively by the bound configurations of the composite nucleus. As with compound reactions, it is imagined that the incident particle is captured by the target nucleus but that emission takes place before the attainment of statistical equilibrium. For MSC reactions, we

also employ the model of Feshbach, Kerman and Koonin [4]. Our implementation of the MSC reaction formalism follows basically the method of Chadwick and Young [25]. The differential MSC cross section is given by

$$\frac{d\sigma}{dE} = \frac{\pi}{k^2}\sum_J (2J+1)[R_{MSC}T_J]\sum_{N=1}^{r}\sum_{\nu l}\frac{\langle\Gamma_{NJ}^{\uparrow\nu l}(U)\rangle}{\langle\Gamma_{NJ}\rangle}\prod_{M=1}^{N-1}\frac{\Gamma_{MJ}^{\downarrow}}{\Gamma_{MJ}}, \tag{29}$$

where T_J is the entrance channel transmission coefficient of spin J, N the reaction stage, $n = 2N+1$ the exciton number, l the orbital angular momentum of the emitted particle, ν designates the emission modes corresponding to $\Delta n = 0, -2$ and $+2$, $\langle\Gamma_{NJ}^{\uparrow\nu l}(U)\rangle$ is the emission width, $\Gamma_{MJ}^{\downarrow}$ the damping width and Γ_{MJ} the total width. Expressions for these widths are given in [25]. All transmission coefficients that appear in the various components of Eq. (29) are calculated with ECIS88, using the same optical model as used in the other reaction mechanisms. Although MINGUS is able to calculate MSC emission up to five steps, in practice it is sufficient to include only two stages and to consider the remainder as r-stage (equilibrium) contribution. For the level density, we use Eq. (23) with B equal to the binding energy to ensure that only bound particle-hole configurations are taken into account.

An important quantity in Eq. (29) is the reduction factor R_{MSC}. Since there is a depletion from the total reaction flux by the collective and MSD contribution, an intuitive guess for this reduction factor would be

$$R_{MSC} = \frac{\sigma_r - \sigma_{dis} - \sigma_{MSD}}{\sigma_r}, \tag{30}$$

where σ_{dis} is the discrete, collective cross section, σ_{MSD} the total MSD cross section and σ_r the reaction cross section. Indeed, the original FKK model uses this reduction factor. This is based on the assumption that as soon as the reaction proceeds through the unbound chain, the configuration will remain unbound until particle emission takes place. One may however imagine that the leading particle loses a large fraction of its initial kinetic energy after one or more successive collisions in a multi-step process. Then, instead of the process of fast emission, some of the particle flux may flow into the bound chain and give rise to (multi-step) compound emission. A practicable method for this P-Q cross-over effect within the FKK theory has been discussed by Chadwick and Young [25] and by Marcinkowski et al. [26]. In our work, we adopt the latter method and introduce a gradual absorption of the flux into subsequent reaction steps on the basis of level density ratios. It is important to note that this P-Q transition model *reduces* the MSC contribution since a significant part of the non-MSD emission flux does not enter the 2p1h MSC-stage from the initial stage but enters the 3p2h MSC-stage from the MSD chain. The predominance of the damping width over the emission width for the 3p2h MSC-stage then implies that this flux almost completely propagates to the equilibration stage, contributing to compound emission rather than MSC emission.

In our MSC calculations, we use constant wavefunctions for the bound states. The item of using either constant or realistic wavefunctions has been subject to a lot of debate [36]. Recently, Kawano [37] has performed MSC calculations with both alternatives and found that the differences in the calculated cross sections were small. This small difference, added to the aforementioned reduced importance of MSC reactions this justifies our use of constant wavefunctions for practical calculations.

7 Evaporation

We describe compound emission by the continuum Hauser-Feshbach formula [2], and include competition by neutrons, protons, deuterons, tritons, ^{3}He, alpha particles and gamma rays. Emission from secondary and higher stages of all these particles is taken into account (provisionally with the Weisskopf-Ewing formula) until all possible outgoing channels are closed. Throughout all multiple emissions, we assume equilibrium processes only, i.e. multiple pre-equilibrium emission is not yet included in this work. As can also be inferred from classical pre-equilibrium models [38], this omission will become important for incident nucleon energies above about 50 MeV. Then, the possibility that a second non-equilibrium particle is emitted is no longer negligible. The first steps to describe this mechanism in a quantum-mechanical way (by means of multiple MSD emission) have been taken by Chadwick et al. [9].

8 Results

The partial reaction models that we have described are all included in the code system MINGUS. The code system consists of three programs. The first program deals with the specification of the basic nuclear reaction information, such as optical model and nuclear structure parametrizations. With this information, all necessary input files for ECIS88 (i.e., the second program) are created. In the third program, the results as provided by ECIS88 are processed into double-differential spectra on the basis of the prescriptions given in this paper.
For the calculations on ^{208}Pb, we use for the level density parameter at the binding energy $a_B = 10.02$ MeV^{-1} and for the pairing energy $P = 1.80$ MeV. For ^{209}Bi, these values are $a_B = 11.72$ MeV^{-1} and $P = 0.26$ MeV. The calculations for ^{209}Bi are based on the same neutron optical model as for ^{208}Pb.
There is only one adjustable parameter in our calculations, namely the l-independent deformation parameter β for the MSD process. In Ref. [39], we published a first attempt to parametrize this constant for (p,p') reactions. For the present version of our model code, we find the parametrization:

$$\beta^2 = c\frac{2.0.10^4}{A^3 E_{lp}\max(10, E_x)}, \tag{31}$$

where E_{lp} is the energy of the leading particle and E_x the excitation energy, both in MeV. The factor c should be rather close to one.
To get insight in the contribution of the several reaction mechanisms, and as a guideline for calculations with energies above 20 MeV, we first analyzed precisely measured experimental double-differential spectra [40] at 14.1 MeV, see fig. 4. The displayed agreement in the collective region confirms that considerable predictive power can be attained by the use of independently obtained deformation lengths, also for the levels beyond the first 3^- and 5^- states. The width of the Gaussians that broaden the discrete state cross sections (see Section 3) has been initialized to 0.4 MeV at the elastic peak. After about 6 MeV of excitation energy the individual states are no longer distinguishable and the MSD mechanism (which for 14 MeV reactions consists almost entirely of one-step direct) gradually takes over. Its predominance just above the discrete region is (at least intuitively) clear: direct processes prevail for outgoing energies near the incident energy, both for discrete excitations and excitations just in the continuum. For the 14 MeV reaction, the MSD parameter of Eq. (31) is $c = 1.2$. Another conspicuous aspect of our results is the minor role played by the MSC process. This is attributed to the P-Q transitions that we have incorporated and is in line with recent work by Chadwick et al. [25] and

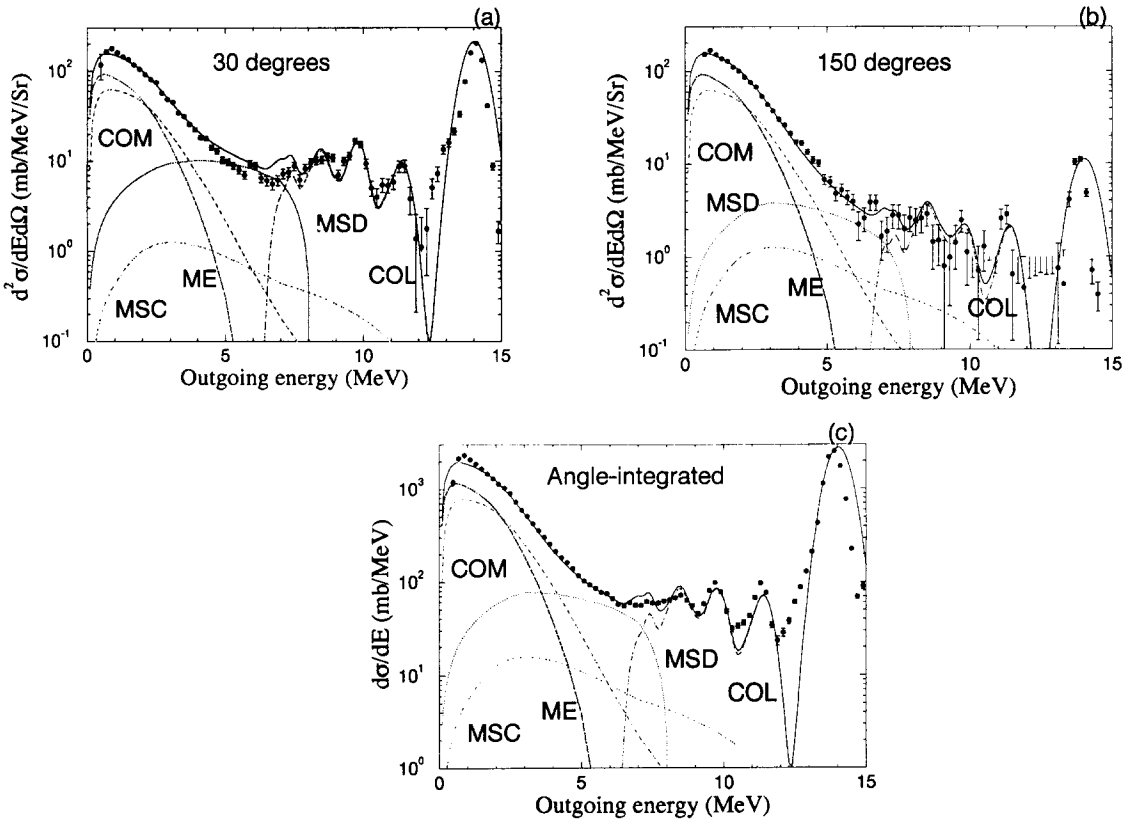

Figure 4: ^{208}Pb(n,xn) cross sections at 14.1 MeV: (a) 30 degrees, (b) 150 degrees and (c) angle-integrated. COL labels the collective cross section, COM the compound contribution and ME multiple emission.

Marcinkowski et al. [26]. We also like to point out that for ^{208}Pb the use of an energy-dependent level density parameter is imperative to inhibit the MSC contribution.

For somewhat higher incident neutron energies, see fig. 5, we see that the high-energy tail becomes longer and is entirely dominated by collective and MSD processes. As discussed in section 3, the agreement between the calculated and measured collective enhancement is independent of incident energy (compare figs. 4 and 5). For the elastic width we have adopted a value of 0.5 MeV for both the 20 MeV and 25.7 MeV reaction. The MSD parameter is $c = 1.1$ for the 20 MeV reaction and $c = 1.25$ for the 25.7 MeV reaction. Since the c-values show little variation between 14, 20 and 25.7 MeV, it seems that for energies up to at least 26 MeV, we can predict angle-integrated and double-differential (n,xn) spectra with good accuracy. Unfortunately, neutron spectra for ^{208}Pb or ^{209}Bi and for incident neutron energies above 26 MeV do not seem to exist.

Next, we turn to the (p,xn) spectra that were considered in the Comparison. Our participating code KAPSIES contributed with (p,p') cross sections below 200 MeV, but was not able to predict (p,xn) spectra. Despite the fact that we now know the experimental data and the results of other codes, we like to present the (p,xn) results of MINGUS for some reactions considered in the exercise. In fig. 6, our calculated spectra for the 25, 45 and 80 MeV (p,xn) reactions on ^{208}Pb are compared with experimental data and, for 25 MeV, with GNASH [3]. For all three incident energies we used $c = 0.9$ for the (p,n) process and $c = 1.8$ for the (p,p') process. In fig. 7, we compare MINGUS-calculations with recent 113 MeV (p,xn) data. For this reaction we used $c = 0.9$ (p,n) and $c = 1.34$ (p,p'). In general, these figures reveal that for high incident proton energies, there is a discrepance just above the evaporation region between the calculations and the experimental data. This is attributed to the possibility of a second fast particle (multiple

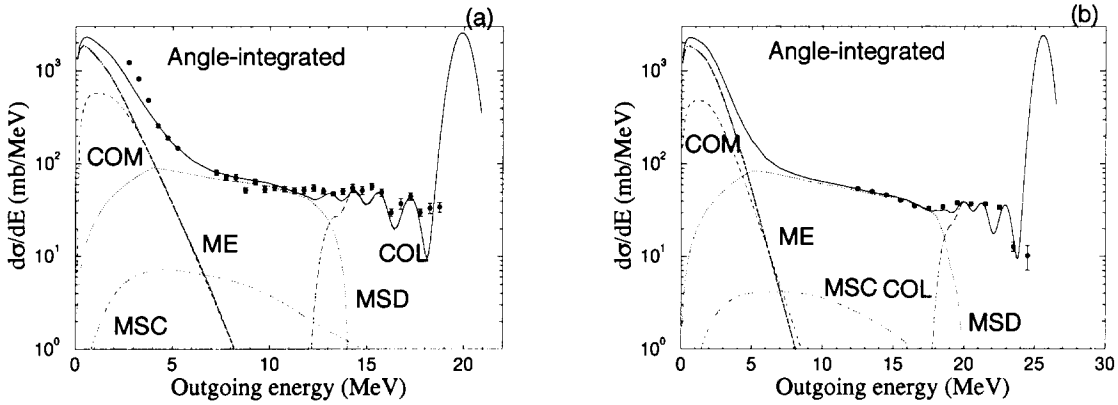

Figure 5: Angle-integrated ^{209}Bi(n,xn) cross sections at (a) 20 MeV and (b) 25.7 MeV. COL labels the collective cross section, COM the compound contribution and ME multiple emission.

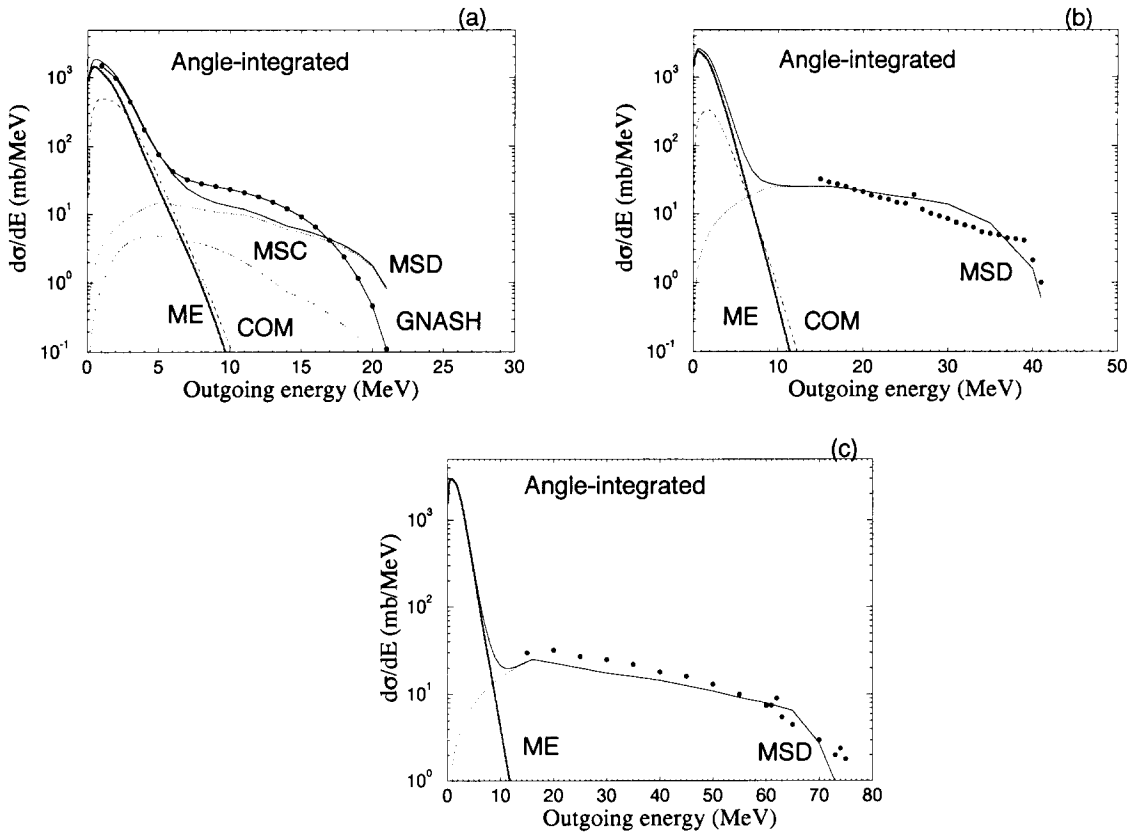

Figure 6: Angle-integrated ^{208}Pb(p,xn) cross sections at (a) 25 MeV (compared with GNASH-results), (b) 45 MeV and (c) 80 MeV. COM labels the compound contribution and ME multiple emission.

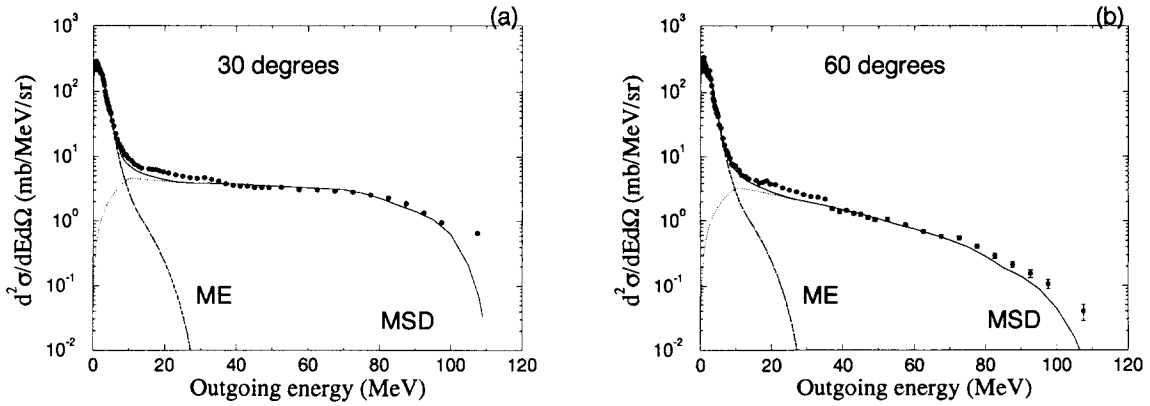

Figure 7: ^{208}Pb(p,xn) cross sections at 113 MeV: (a) 30 degrees and (b) 60 degrees. ME labels multiple emission.

MSD emission). Also, at the highest outgoing energies, we underestimate the experimental data. Probably this stems from discrete (p,n) reactions that we have not yet taken into account.

9 Nuclear data evaluation

The computer code as described in this paper, as well as many of the other codes participating in the Comparison, has two basic purposes. First, there is the iterative process of comparing calculations with experimental data (and the results of other codes) and updating the implemented physics. Once a satisfactory state of this first phase has been attained, we can proceed with the next stage and use the code for the evaluation of nuclear data files, thereby providing the closest possible connection between nuclear physics and applied calculations. Given the scarcity of measured cross sections for energies above 20 MeV, it is obvious that an evaluated file above 20 MeV should consist mainly (if not completely) of *calculated* data. A recommended procedure is to tune the adjustable parameters of the model with the help of the few experimental data sets that do exist. Subsequently, one can produce the nuclear data file using repeated calculations on an appropriate energy grid, with the determined parameters.
An evaluation of the nuclide ^{208}Pb is interesting, since lead is regarded as a promising candidate to serve as a target material in accelerator-based transmutation concepts. Recently, we investigated the nuclear data needs for accelerator-based transmutation of waste [41] and tentatively proposed a high-priority list for cross sections to be included in future evaluated files. Also, we provisionally set the upper energy limit of the data file at 100 MeV, *assuming that for higher energies the intranuclear cascade models are adequate.* Although some additions (notably multiple pre-equilibrium emission) and improvements in our model code are still required, we have created a 100 MeV proton file with MINGUS using the physical parameters as described in the previous section and according to the format proposals made in Ref. [42]. The output of MINGUS is automatically transformed into ENDF-6 formatted data and in this way a file containing elastic, reaction, (p,xn), (p,xp) and transmutation cross sections is obtained.
The directory of the data file is displayed in table 1. For proton elastic scattering, we provisionally have used (following [43]) the "nuclear + interference" expansion (LAW=5, LTP=12) for the representation of the cross section. However, this option entails some arbitrariness in the choice of the cut-off angle since both the Coulomb and the interference term display singular behavior in the vicinity of zero degrees. Therefore, the option of a renormalized Legendre expansion (LTP=2) is presently under investigation [44]. In Ref. [42], we have argued that for intermediate energies the large number of open channels no longer enables to maintain the conventional

Table 1: Directory of proton data file to 100 MeV for ^{208}Pb (in ENDF-6 format).

MF	MT	Description
1	451	General information
3	2	Elastic cross section
3	5	(p,anything) cross section
6	2	Elastic angular distribution
6	5	(p,anything) yields and energy-angle distributions

classification for the partial reaction cross sections. Therefore, all non-elastic processes have been lumped in MT5, so that MF6/MT5 now contains the total reaction cross sections. Although in principle we have the possibility to store the cross sections of the discrete levels separately, we use the continuum representation for the whole outgoing spectrum (If future applications require the former alternative, we can always use discrete storage). In MF6/MT5, we first give the neutron and proton yields and subsequently the energy-angle distribution as a tabulated function (LANG=12). As an alternative option, we may also choose the more compact Kalbach expansion (LANG=2) by specifying the (multi-step) compound fraction of the reaction that is provided by MINGUS. With this choice, we would overrule the double-differential multi-step direct calculation. Finally, we have filled MF6/MT5 with the yields of the product nuclides using LAW=0. This can be combined with MF3/MT5 to give the transmutation cross sections.
The evaluation (or better, creation) of the data file that we just described is completely automatized. This entails that future improvements of the physics in MINGUS can immediately be paralleled by an updated data file.

10 Conclusions

We have presented calculated results for ^{208}Pb using the computer code MINGUS, which integrates elastic, collective, MSD, MSC and compound cross sections. We use a dispersive optical model for neutrons and include many discrete levels for the DWBA calculation of the collective cross section. The nucleon optical models for ^{208}Pb are well tested and describe the whole energy region up to at least 150 MeV with good accuracy. Our approach to include as many discrete levels as possible and subsequently to calculate their separate contributions to the spectra gives a good prediction of the fluctuating high-energy tails and enables to handle the overlap with the continuum properly. For the pre-equilibrium part of the reaction, we use the MSD/MSC model of FKK, including the P-Q transition processes that reduce the importance of MSC reactions. To maintain consistency with compound reaction models, we renormalized the particle-hole state densities for the pre-equilibrium models. Our computational model contains one adjustable parameter, namely the l-independent deformation parameter β for the MSD reaction. To some extent, we have the systematics of β under control, but more tests against measurement are required. For incident energies above about 50 MeV, multiple pre-equilibrium emission needs to be included. We plan this as future work. For the evaporation part, the Hauser-Feshbach model is employed for primary emission and the Weisskopf-Ewing model for multiple emission. The same energy-dependent level density parameters are used in both the partial and total level density models. We have compared our calculations with several

experimental data sets, among others those that were considered in the Comparison. Finally, we have created a 100 MeV proton data file with MINGUS-calculations.
In the future, we plan to extend MINGUS with other physical models, in order to describe phenomena such as multiple pre-equilibrium emission, the excitation of giant resonances, pre-equilibrium gamma ray emission and fission. Simultaneously we will focus on the associated evaluation aspects.

Acknowledgements

The authors wish to thank J. Raynal and M.B. Chadwick for helpful discussions. One of the authors (A.K.) wishes to thank the CEA for the kind hospitality during his visit in Bruyères-le-Châtel.

References

[1] G. R. Satchler, *Direct Nuclear Reactions*, Oxford University Press (New York, 1983).
[2] E. Gadioli and P.E. Hodgson, *Pre-equilibrium nuclear reactions*, Oxford University Press 1992.
[3] M. Blann, H. Gruppelaar, P. Nagel and J. Rodens, "International Code Comparison for Intermediate Energy Nuclear Data", NEA Data Bank report, 1994.
[4] H. Feshbach, A. Kerman and S. Koonin, Ann. Phys. **125**, 429 (1980).
[5] T. Tamura, T. Udagawa and Lenske, Phys. Rev. **C26**, 379 (1982).
[6] R. Bonetti, M. Camnasio, L. C. Milazzo and P. E. Hodgson, Phys. Rev. C **24**, 71 (1981).
[7] *Multistep Direct Reactions*, Faure, South Africa (30 Sep-2 Oct 1991), ed. R.H. Lemmer, World Scientific (1992). See contributions by H. Feshbach, P.E. Hodgson and A.J. Koning.
[8] R. Bonetti, A.J. Koning, J.M. Akkermans and P.E. Hodgson, to appear in Phys. Rep. (1994).
[9] M.B. Chadwick, P.G. Young, D.C. George and Y. Watanabe, submitted to Phys. Rev. C; M.B. Chadwick, personal communication.
[10] J. Raynal in *Applied nuclear theory and nuclear model calculations for nuclear technology applications*, Trieste, 15 Feb-19 March, 506 (1988).
[11] A.J. Koning and J.M. Akkermans, Phys. Rev. **C47**, 724 (1993).
[12] C. Mahaux and H. Ngô, Nuc. Phys. A**378**, 205 (1982).
[13] C. Mahaux, H. Ngô and G.R. Satchler, Nuc. Phys. A**449**, 354 (1986).
[14] P.E. Hodgson in *Applied nuclear theory and nuclear model calculations for nuclear technology applications*, Trieste, 15 Feb–19 March, 1988, p. 1.
[15] J.P. Delaroche, private communication.
[16] C.H. Johnson, D.J. Horen and C. Mahaux, Phys. Rev. **C36**, 2252 (1987).
[17] R.W.Finlay, W.P. Abfalterer, G.Fink, E. Montei, T. Adami, P.W. Lisowski, G.L. Morgan, R.C. Haight, Phys. Rev. **C47**, 237 (1993).
[18] J.P. Delaroche, in Proceedings of the International Symposium on *Nuclear Data Evaluation Methodology*, ed. C.L. Dunford, October 12-16 1992, Brookhaven, USA, p. 347.
[19] J.-P. Delaroche and C. Liegeois, CEA Bruyères-le-Châtel, internal report.
[20] W.T. Wagner, G.M. Crawley, G.R. Hammerstein and H. McManus, Phys. Rev. **C12**, 757 (1975).
[21] D.E. Bainum, R.W. Finlay, J. Rapaport, J.D. Carlson and W.G. Love, Phys. Rev. **C16** 1377 (1977).
[22] T.S. Cheema and R.W. Finlay, Phys. Rev. **C37**, 910 (1988).

[23] R.E. Shamu and P.G. Young, J. Phys. G **19**, L169 (1993).
[24] H. Kalka, M. Torjman and D. Seeliger, Phys. Rev. **C40** 1619 (1989).
[25] M.B. Chadwick and P.G. Young, Phys. Rev. **C47**, 2255 (1993).
[26] A. Marcinkowski, J. Rapaport, R.W. Finlay, C. Brient, M. Herman and M.B. Chadwick, Nucl. Phys. **A561** 387 (1993).
[27] U. Facchini and E. Saetta Menichella, Energ. Nucl. **15**, 54 (1968).
[28] A.V. Ignatyuk, G.N. Smirenkin and A.S. Tishin, Sov. J. Nucl. Phys. **21**, no. 3, 255 (1975).
[29] W.D. Myers and W.S. Swiatecki, Ark. Fysik **36**, 593 (1967).
[30] W. Dilg, W. Schantl, H. Vonach and M. Uhl, Nucl. Phys. A **217**, 269 (1973).
[31] F. C. Williams, Nucl. Phys. A **166**, 231 (1971).
[32] J.M. Akkermans and H. Gruppelaar, Z. Phys. **A321**, 605 (1985).
[33] P. Obložinský, Nuc. Phys. **A453**, 127 (1986).
[34] H. Nishioka, H.A. Weidenmüller and S. Yoshida, Ann. Phys. (NY) **183**, 166 (1988).
[35] A.J. Koning and J.M. Akkermans, Ann. Phys. (NY) **208**, no.1, 216 (1991).
[36] R. Bonetti, M.B. Chadwick, P.E. Hodgson, B.V. Carlson and M.S. Hussein, Phys. Rep. **202**, no. 4, 171 (1991).
[37] T. Kawano, Kyushu University, unpublished.
[38] J.M. Akkermans and H. Gruppelaar, Z. Phys. **A300**, 345 (1981).
[39] A.J. Koning, in Symposium on *Nuclear Data Evaluation Methodology*, Brookhaven National Laboratory, Upton, New York, Oct. 12–16 1992, p. 434.
[40] A. Takahashi, J. Nucl. Sc. Techn. **26** 15 (1989) and references therein.
[41] A.J. Koning, "Review of High Energy Data and Model Codes for Accelerator-Based Transmutation", NEA Data Bank Report NEA/NSC/DOC (92) 12.
[42] A.J. Koning, "Requirements for an Evaluated Nuclear Data File for Accelerator-Based Transmutation", NEA Data Bank Report NEA/NSC/DOC(93) 6.
[43] P.G. Young, E.D. Arthur, M. Bozoian, T.R. England, G.M. Hale, R.J. LaBauve, R.C. Little, R.E. Macfarlane, D.G . Madland, R.T. Perry and W.B. Wilson, "Transport data libraries for incident proton and neutron energies to 100 MeV", Los Alamos National Laboratory, report LA–11753–MS (1989).
[44] J. Raynal, private communication.